



# Production of High Surface Area Activated Carbon from Peanut Shell by Chemical Activation with Zinc Chloride: Optimisation and Characterization

Ashleigh Fletcher<sup>1</sup> · Tosin Somorin<sup>1</sup> · Oluwagbemi Aladeokin<sup>1</sup>

Received: 20 July 2023 / Accepted: 21 September 2023 / Published online: 3 October 2023  
© The Author(s) 2023

## Abstract

The potential of peanut shell as a precursor to produce activated carbon by chemical activation with  $\text{ZnCl}_2$ , and the effect of activation variables were investigated using response surface methodology. Activation variables examined were temperature, hold time and impregnation ratio; among these, impregnation ratio and temperature were found to most affect the final characteristics of the produced activated carbon. The activation process was mapped, using design of experiments, and the optimum activation conditions were found to be a temperature of 485 °C, with a hold time of 15 min and an impregnation ratio of 1.7. Under the optimised conditions, an activated carbon with a relatively high surface area of ~ 1700 m<sup>2</sup>/g was produced, at a yield of 47%. Moreover, the carbon exhibited a relatively high density, ranging from 1.455 g/cm<sup>3</sup> to 1.750 g/cm<sup>3</sup>, as well as a low ash content below 1% and a high fixed carbon content above 86%. SEM analysis and FTIR characterisation revealed the heterogenous nature of the produced carbon materials. The developed materials, with potential as adsorbents, removed up to 99.8% of a target dye (methyl orange) depending on their available surface area. Hence, through the insights gained, an optimised carbon is produced, demonstrating the potential to tailor activated carbon materials produced from waste biomass.

**Keywords** Chemical activation · Activated carbon · Peanut shell · Impregnation ratio · Response surface methodology

## Introduction

In the last decade, global peanut cultivation has grown due to increased demand, attributed mainly to their perceived health benefits, resulting in a total production of ~ 41.4 MMT in 2019/2020 [1]. Peanut and other nutshells are considered as waste in various parts of the world and are usually used for their fuel value [2]. However, this agricultural by-product can be converted to higher value products, such as activated carbon (AC) [3, 4], which has various commercial applications and is typically produced from different organic precursors such as wood, coconut shell, coal, bones, peat etc. [5, 6]. In addition, various agricultural residues, such as rice husk, corn stalks, apricot stones, almond shells, coffee beans etc., have been explored to

produce ACs, due to their comparatively low cost [7, 8]. Researchers have previously reported the production of AC using peanut shell as a precursor [3, 9–13], with surface areas up to 1200 m<sup>2</sup>/g reported; however, these studies have lacked a focus on determining the controlling variables to enhance the carbon characteristics.

AC forms a large class of porous solid media, and due to their large porosities, they are widely used as adsorbents in the removal of pollutants and organic compounds from gases, water, wastewater, and air [14]. The textural and structural characteristics of AC depend on factors such as carbon content and solid structure of the precursor, activation method, activating agent and activation conditions. AC can be obtained via two routes: physical and chemical activation. Physical methods involve carbonisation of biomass in an inert environment, followed by partial gasification of the resulting char in oxidising gases such as carbon dioxide, steam, air or a mixture of these gases, using high temperatures, ranging between 700 and 1000 °C, to enhance the pore structure [5, 15, 16]. By contrast, chemical methods require lower temperatures (< 700 °C), using dehydrating

✉ Oluwagbemi Aladeokin  
oluwagbemi.aladeokin@strath.ac.uk

<sup>1</sup> Department of Chemical and Process Engineering,  
University of Strathclyde, Glasgow G1 1XJ, UK

agents such as  $\text{ZnCl}_2$ , phosphoric acid, KOH, etc., to influence carbonisation and inhibit the formation of tar, thus increasing the carbon yield [16]. Such chemical routes are mostly applied for biomass with carbon content above 45%, [17] and peanut shells are reported to have levels at ~46% [2], making them ideal candidates for chemical activation. The effectiveness of  $\text{ZnCl}_2$  in enhancing the porosity of porous carbonaceous materials has been well established in previous studies.  $\text{ZnCl}_2$  acts as a catalyst that decomposes the biomass structure and facilitates the dehydration process during the carbonisation step, leading to the formation of char, aromatic compounds and pore structure [15, 16, 18]. Therefore, this study employs  $\text{ZnCl}_2$  as the chemical agent for the preparation of porous carbon materials.

As ACs can be applied in a range of applications, it is essential to tailor the final properties of the AC to the chosen application, to fully understand and optimise the process [19]. Traditional approaches involve varying each experimental parameter, one at a time; however, a more efficient way to reduce the number of experimental runs, while also understanding the interplay between variables, is to apply design of experiment (DoE) [20], which provides the capability to vary factors simultaneously. Response surface methodology or modelling (RSM) is a useful technique used in DoE to study the interactions between parameters, allowing optimisation. It employs various surface visualisation techniques, such as contour plots, surface plots, interaction plots, and so on, to evaluate the influence of the factors on the response and the identification of the optimal factor combination that maximises or minimises the response [21].

Previous studies have investigated the effect of various activation parameters, such as impregnation ratio, temperature, time, and particle size, on the preparation of porous carbon materials from different precursors [15, 22–24]. Among these parameters, impregnation ratio and temperature were found to have a significant influence on the characteristics of the final product. However, studies of peanut shells did not provide sufficient information on how the activation variables influenced the final properties of the produced carbons and the optimisation of the activation variables. Moreover, previous studies of peanut shells employed two stages to carbon production: precursor charring and chemical activation shells [3, 10]. This process is complex and energy-intensive, compared to the one-stage process.

In this work, RSM was used to study the influence of activation variables in a single step chemical activation process, selected to simplify the process for production at scale, while providing economic gain, as energy input is reduced. Through the insights gained, an optimised carbon is produced, demonstrating the potential to tailor AC materials produced from waste biomass.

## Materials and Methods

### Materials

Raw peanut (enclosed in its shell) was obtained from a commercial source within the UK. Zinc chloride ( $\text{ZnCl}_2$ , > 98%, solid), and 1 M hydrochloric acid (HCl) solution were purchased from Fisher Scientific, UK. Methyl orange ( $\text{C}_{14}\text{H}_{14}\text{N}_3\text{NaO}_3\text{S}$ ) was purchased from Sigma – Aldrich, UK. All reagents used were of analytical grade and were used without further purification.

### Preparation of Activated Carbons

The peanut shells (PNTS) were removed and washed with water to remove any surface dirt before subsequent oven-drying at  $100 \pm 2$  °C overnight. After drying, the shells were ground and screened to a particle size of 2 mm with a sieve shaker. 5 g (W1) of the screened precursor was impregnated with  $\text{ZnCl}_2$  at various impregnation ratios ( $\text{ZnCl}_2$  g/ precursor g) of 0.25, 1.13 and 2. In all experiments, the precursor was properly mixed in 25 mL of deionised water containing different weights (W2) of  $\text{ZnCl}_2$  depending on the impregnation ratio. The mixture was allowed to equilibrate for ~24 h under room temperature. After the impregnation process, the sample was oven-dried at  $100 \pm 2$  °C overnight. The oven-dried sample was carbonised in the tube furnace under nitrogen (inert atmosphere, 250 mL/min), at a temperature of 300, 450 or 600 °C using a dwell/hold time (residence time) of either 15, 68 or 120 min at a ramp-rate of 15 °C/min. The carbonised product obtained from the furnace was weighed (W3), before being transferred into a jar containing 200 mL of 0.1 M HCl and agitated for 1 h on a shaker to leach out any remaining activating salt. The product was boiled in hot deionised water for ~10 min and washed in room temperature deionised water to completely remove any chloride ions and reduce acidity. The washed product was dried in the oven at  $100 \pm 2$  °C for ~24 h, weighed again after drying (W4) and stored for characterisation. The naming of samples for easy identification includes the precursor initials, impregnation ratio (I.R.), activation temperature and hold time.

The yield of the process in percentage was calculated using the following equation:

$$\text{Yield} = (W4/W1) \times 100 \quad (1)$$

Also, to take account of the activating reagent recoverable from washing, the following equation is used to calculate the reagent recovery (R.R.) in percentage:

$$R.R. = ((W3 - W4)/W2) \times 100 \quad (2)$$

## Design of Experiment for Activated Carbon Preparation

In this study, Design Expert (V13.1.0. Stat-Ease Inc., Minneapolis, USA), a statistical software, was used to set the activation variables/factors' values. Face-centred CCD (FCCD) with three factors and levels design was employed to provide maximum information in minimum experimental runs. This design type is used to find best values for a set of factors to give an optimal response [25]. The factors investigated in this design were temperature (A), hold time (B) and I.R. (C), based on preliminary studies and previous reports [22, 23, 26]. Randomised experimental runs were used to minimise the effects of factors that cannot be controlled in the process. The coded values for the activation variables were – 1 for minimum, 0 for centre point and + 1 for maximum point, as shown in Table 1. Yield ( $Y_1$ ) and surface area ( $Y_2$ ) are important properties in determining the economic viability and adsorption capability of ACs, respectively. These two properties were considered as the responses in the design.

## Materials Characterisation

### Proximate Analysis

Proximate analysis of the raw precursor and the activated carbon was carried out using a thermogravimetric technique version of British Standard BS1016. The procedure was carried out using a method similar to that reported by Ottaway [27]. A NETZSCH STA 449 F3 Jupiter system was used for this analysis.

### Adsorption Experiment

Adsorption experiments were carried out to evaluate the efficiency of the activated carbon, by agitating 0.05 g sample with 50 mL of methyl orange (MO) solution (100 mg/L), in 500 mL Erlenmeyer flasks. The mixtures were agitated on an orbital shaker operated at 150 rpm, and at room temperature. At predetermined time intervals,

the mixtures were separated by centrifugation, and the residual concentrations ( $C_t$ ) were measured at 465 nm, using a Varian CARY 5000 UV-VIS-NIR spectrophotometer. The percentage removal of MO was calculated using the equation below.

$$\text{Removal (\%)} = \frac{C_0 - C_t}{C_0} \times 100 \quad (3)$$

Where  $C_0$  and  $C_t$  (mg/L) represent the initial concentration and concentration at time  $t$ , respectively.

### Point of Zero Charge

The determination of point of zero charge (PZC) of the AC was carried out using a salt addition method [28]. Several vials containing an aliquot of 40 mL of 0.1 M  $\text{NaNO}_3$  each were prepared. 0.1 M  $\text{HNO}_3$  or 0.1 M  $\text{NaOH}$  solutions was used to adjust the pH values from 3 to 11. 0.2 g of AC was added to each of the solutions and the solutions agitated at 150 rpm for ~ 24 h on a VWR STD 3500 shaker. After equilibrium was attained, the mixture was filtered, and the pH reading was recorded. The experiment was performed in triplicate and a mean value recorded.

### Fourier Transform Infrared Spectroscopy

AC samples were analysed for various surface functional groups using Fourier transform infrared spectrometry (FTIR). The samples were scanned over a range of 500–4000  $\text{cm}^{-1}$  using an MB3000 FT-IR laboratory analyser with Horizon MB™ FTIR software. 449 scans were taken at a resolution of 8  $\text{cm}^{-1}$ .

### Density

Densities of the AC samples created within this study were determined using helium pycnometry (Micromeritics Accupyc II helium pycnometer with Accupyc II version 3.0 software). A pycnometer sample cup was cleaned and

**Table 1** Activation parameters and their coded values for the Face-centred central composite design for chemically activated synthesis of peanut shell derived carbons

Variables (factors)	Units	Variable levels				
		Low (-1)	Mid (0)	High (1)	$-\alpha$	$+\alpha$
Temperature (A)	(°C)	300	450	600	300	600
Hold time (B)	(min)	15	68	120	15	120
Impregnation ratio, I.R. (C)	(wt/wt)	0.25	1.13	2	0.25	2
Responses						
Yield ( $Y_1$ )	(%)					
Surface area ( $Y_2$ )	( $\text{m}^2/\text{g}$ )					

**Table 2** Model summary statistics for analysed variables for chemically activated carbons derived from peanut shells

Response	$R^2$	Adjusted $R^2$	Predicted $R^2$	Std. Dev.	Mean	C.V. %	Adeq. Precision
Yield (%)	0.9932	0.9856	0.9360	0.83	51.26	1.61	33.55
Surface area (m <sup>2</sup> /g)	0.9784	0.9541	0.8475	144.34	926.15	15.58	16.54
Reagent recovery (%)	0.9833	0.9645	0.7697	5.00	70.83	7.07	21.70
Micropore area (m <sup>2</sup> /g)	0.9793	0.9561	0.8616	69.63	469.49	14.02	16.88
Mesopore area (m <sup>2</sup> /g)	0.9694	0.9350	0.7634	99.35	429.82	23.11	15.77

weighed before a small sample of AC was introduced into the sample cup; the weight was taken again to determine the sample mass. The sample cup, with the sample, was transferred into the pycnometer, and sealed within the pycnometer for analysis. The system was purged with helium gas to remove any gas molecules trapped within the system before the analysis.

### Textural Analysis

The textural characteristics of the activated carbon were determined using the method of Brunauer et al. [29]. This was achieved using a Micromeritics ASAP 2420 instrument that employs nitrogen adsorption at -195.8 °C. The sample was first degassed before analysis, to remove any contaminant species, via heating under vacuum. Degassing was performed at 250 °C for 4 h, using a ramp rate of 10 °C/min. The specific surface area ( $S_{\text{BET}}$ ) was calculated using Brunauer-Emmett-Teller (BET) method. The micropore area ( $S_{\text{micro}}$ ) and micropore volume ( $V_{\text{micro}}$ ) were obtained the by t-plot method of de Boer et al. [30]. The pore-size distribution was calculated by the Barrett–Joyner–Halenda (BJH) equation [31].

The total pore volume (TPV) was calculated using the equation below.

$$TPV = Q_{\text{sat}} * \left( \frac{\rho_{\text{vap}}}{\rho_{\text{liq}}} \right) \quad (4)$$

Where  $Q_{\text{sat}}$  is maximum nitrogen adsorption (in cm<sup>3</sup>/g, usually at relative pressure of 0.97 or above),  $\rho_{\text{vap}}$  is density of N<sub>2</sub> vapour at STP and  $\rho_{\text{liq}}$  = density of liquid N<sub>2</sub> at boiling point.

### Scanning Electron Microscopy (SEM)

The surface morphology of the raw precursor and the activated carbon was observed, using a JEOL JSM-IT100 scanning electron microscope, at an accelerating voltage of 20 kV. The samples were mounted on aluminum SEM specimen stubs, by double sided carbon adhesive discs. The scanning was performed under high vacuum (HV) and at a magnification of 250x.

## Results and Discussion

### Fit Summary for the Design of Experiment for AC Preparation

Design Expert was used to analyse the dataset obtained from the surface area analysis, yield of the process, and other dependent variables. The sequential model sum of squares from the statistical software suggested quadratic models for all the dependent variables. The regression equations obtained for each dependent variable from the analyses are shown in Eqs. 5 and 6. The coefficient of determination ( $R^2$ ) was used to assess how well the regression model fits the data for this study.  $R^2$  values obtained were 0.9932 and 0.9784 for yield and surface area, respectively. These values indicate a good fit of the dataset to the regression models i.e., above 97% of the variability observed in the responses can be explained by the selected model. The model and fit statistics for all analysed variables are summarised in Table 2. The Adjusted  $R^2$  is a measure of the amount of variation around the mean which can be explained by the model and adjusted for the number of terms in the model. Reduced adjusted  $R^2$  values are observed from the model summary statistics; this may be attributed to the presence of some model terms that do not add much value to the model. The predicted  $R^2$  measures the amount of variation in predictions and can be explained by the model.

$$Y_1 = + 124.50 - 0.25A - 0.05B - 8.07C + 0.01AC - 0.01BC + 1.00C^2 \quad (5)$$

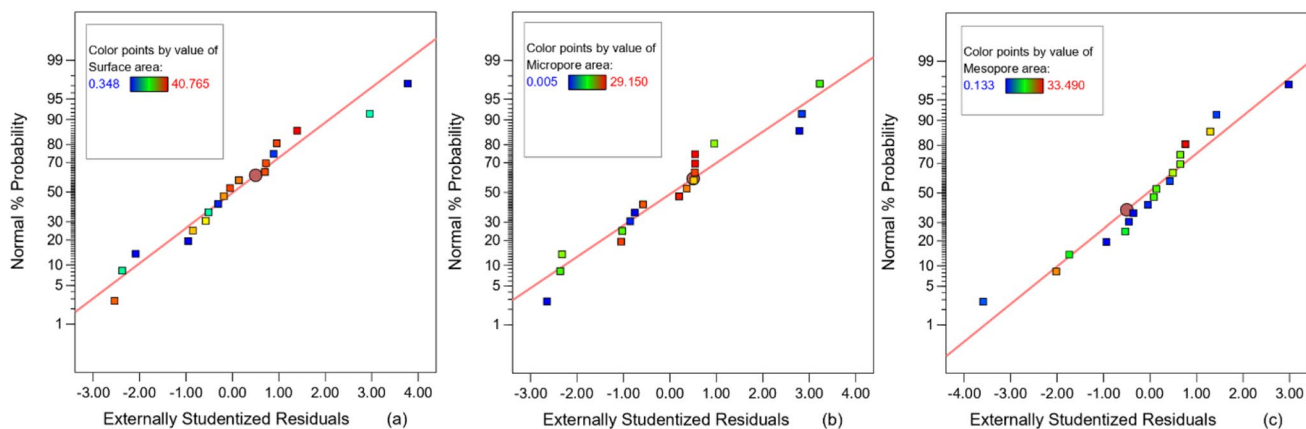
$$Y_2 = - 6429.31 + 29.84A - 2.48B + 367.17C - 0.0039AB + 1.90AC - 0.15BC - 0.0313A^2 + 0.0346B^2 - 380.30C^2 \quad (6)$$

where A = temperature, B = hold time, and C = I.R.

The predicted  $R^2$  values are in reasonable agreement with the adjusted  $R^2$ , i.e., they are within 0.2 of the adjusted  $R^2$ . Within the Design Expert system, an adequate precision > 4 indicates an adequate model discrimination [32]; in this case, all adequate precision values are well above 4. The coefficient of variation (C.V.) is the standard variation

**Table 3** Model summary statistics for responses (after model transformation) for chemically activated carbons derived from peanut shells

Response	$R^2$	Adjusted $R^2$	Predicted $R^2$	Std. Dev.	Mean	C.V. %	Adeq. Precision
Surface area ( $\text{m}^2/\text{g}$ )	0.9937	0.9865	0.9112	1.82	26.34	6.91	30.99
Micropore area ( $\text{m}^2/\text{g}$ )	0.9950	0.9893	0.9158	1.15	19.47	5.92	34.45
Mesopore area ( $\text{m}^2/\text{g}$ )	0.9870	0.9724	0.8781	1.98	17.19	11.53	23.38

**Fig. 1** Normal plots for: **a** surface area **(b)** micropore area **(c)** mesopore area, after model transformation, for chemically activated carbons derived from peanut shells

expressed as a percentage of the mean; this can be used to measure the reproducibility of a model and as a general rule, a model will be reasonably considered reproducible if C.V. is  $> 10\%$  [33]. As shown in Table 2, C.V. for surface area, micropore and mesopore areas are  $> 10\%$ . This can be attributed to errors in the measurement of these quantities.

To further assess the adequacy of the models, diagnostic plots, such as the normal plot, residual versus predicted response plot, and predicted versus actual plot, were employed. The diagnostic plots for yield and surface area are presented in (Figs. S1 and S2, see Supplementary Information). The predicted versus actual plot for yield indicates a strong agreement between the predicted and the actual values, as shown by the points aligning with the 45-degree line and the high  $R^2$  value. On the other hand, the surface area shows a weaker agreement. The normal plot for yield demonstrates that the residuals follow a normal distribution, as evidenced by the points conforming to the straight line. However, for surface area, some departure from the line is noticeable – this suggests that a transformation may enhance the model. The residual versus predicted values plot for yield displays a random distribution of the residuals. The plot should exhibit a random distribution (constant variance of residuals throughout the graph) [34]. Conversely, the same plot for surface area exhibits some heteroscedasticity, as the variance of the residuals increases from right to left. This may indicate the need to transform the response. No outlier was found in any of the plots.

As indicated by the adjusted  $R^2$  values for surface area, micro- and mesopore areas, reducing the number of terms in the models might improve the adjusted  $R^2$ . Model reduction was performed for the responses by eliminating insignificant terms, after which, the overall models did not show significant improvement (Table S1, see Supplementary Information), possibly because the number of significant terms was higher than that of insignificant terms.

The residual versus predicted values plot indicated that model transformation was necessary. Transformation of responses is an essential aspect of any data analysis. It is required when the residuals (errors) are dependent on the magnitude of the predicted values [35]. Model transformation was carried out by using the recommended transformation, square root transformation, within Design Expert. The square root transformation is the simplest form of transformation; this was employed to enhance the model. The model summary statistics after model transformation are shown in Table 3. The  $R^2$ , and adjusted  $R^2$ , values increased, and the predicted  $R^2$  remained reasonably consistent with the adjusted  $R^2$  values. This indicates a better fit, reducing the errors between the observed values and the predicted values.

Figure 1 displays the normal plots for the responses. The enhancement of the models, after transforming the responses, is further verified by the increased conformity of the residuals on the normal plots, for all responses.

Equation 7 shows the final regression equation (Table S3, Supplementary Information) for the ANOVA performed for surface area response after transformation.

$$\begin{aligned} \sqrt{Y_2} = & -158.93 + 0.73A + 0.037B + 11.86C - 0.00016AB \\ & + 0.022AC + 0.018BC - 0.00072A^2 + 0.00025B^2 \\ & - 7.35C^2 \end{aligned} \quad (7)$$

## Analysis of Variance (ANOVA)

Statistical analysis was carried out on the independent variables (A: Temperature, B: Hold time, C: I.R.) to observe the single and interaction effect of the variables on the responses ( $Y_1$ : Yield,  $Y_2$ : Surface area) and choose the best model for the system. As presented in Table 3 above, the closeness of  $R^2$  to unity, indicates a good fit of the dataset to the models. However, analysis of variance (ANOVA) was used to further check the adequacy of the selected quadratic models. This was done by comparing the p-values and F-values from the ANOVA table (Table S2, see Supplementary Information). A suitable model will have high F-value, its p-value  $< 0.05$  (significant) and have lack of fit as non-significant ( $p > 0.05$ ) [36]. The analysis shows that the p-values for the quadratic models selected for yield and surface area are  $< 0.05$ . This indicates statistical correctness of the selected models.

It is observed from the table that model terms A, B, C, AC, and  $A^2$  have p-values  $< 0.05$  for yield, i.e., temperature, hold time, I.R., and the interaction of temperature and I.R. affect the yield of the process. Temperature has the greatest impact on yield since it shows the highest F-value, 933.85. The lack of fit is not significant in this case since it shows a p-value  $> 0.05$ . It is observed from the ANOVA table that model terms A, C, AC,  $A^2$ , and  $C^2$  have p-values  $< 0.05$  for surface area i.e., temperature, I.R., and the interaction of temperature and I.R. are parameters that affect the surface area. Temperature is also observed to have the greatest impact on surface area since it has the highest F-value of 623.98. The lack of fit for this model has p-value  $> 0.05$  i.e., lack of fit is not significant for this model. This indicates that the model fits the dataset and can be used to navigate through the design space.

## Influence of Activation Variables

The one factor effect on the yield of the process is shown in (Fig. S3, see Supplementary Information). The yield reduces with increase in temperature to  $\sim 550^\circ\text{C}$  and above this temperature, the yield only demonstrates a slight decrease. This can be attributed to the basic structure being already formed at  $\sim 500^\circ\text{C}$ , since the distillation of tar occurs  $\sim 350\text{--}500^\circ\text{C}$  [19]. The hold time has little effect on the yield of the process.

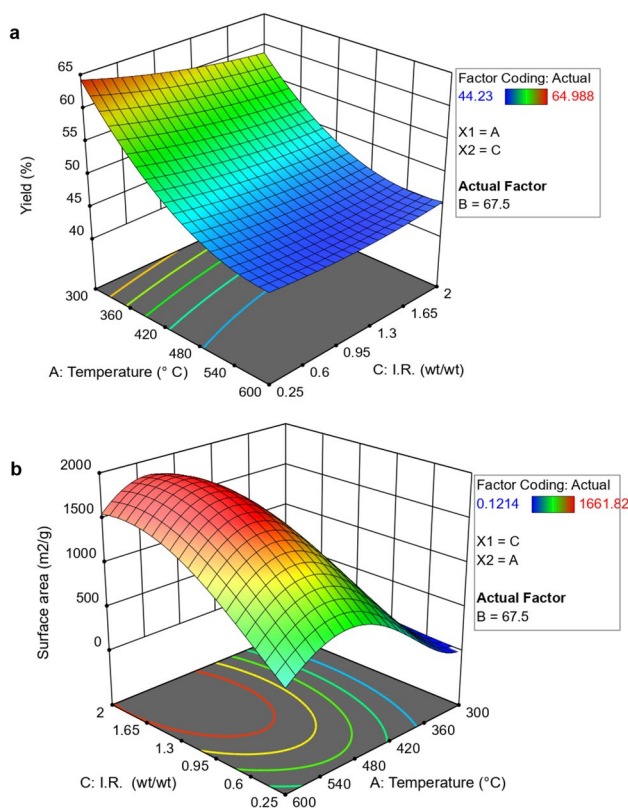


**Fig. 2** **a** Interaction effects of temperature and impregnation ratio (I.R.) on process yield; **b** Interaction effects of temperature and impregnation ratio (I.R.) on surface area, for chemically activated carbons derived from peanut shells

The yield demonstrates a gradual reduction as I.R. increases, showing minor changes for I.R.  $> 1.5$ . Increase in activating agent may lead to more cracks in the structure, causing deformation of micropores and reducing productivity [37]. An increase in activating agent increases the evolution of volatile matter, which leads to a reduction in yield [5]. The interaction of temperature and I.R. is also an important factor that affects the yield of the process. As shown in Fig. 2a, at temperatures  $< 350^\circ\text{C}$  and I.R.  $< 1.5$ , the yield of the process is  $\geq 60\%$ , however, the surface area stays below  $500\text{ m}^2/\text{g}$ . The yield remains within the range  $50\text{--}55\%$  at temperatures of  $350\text{--}455^\circ\text{C}$  and is not greatly affected above  $480^\circ\text{C}$ . It is also noted that the surface area increases gradually in this region with increase in temperature; this confirms the significance of temperature in developing the internal porous structure of the carbons. As reported by Hock et al. [17], the formation of pores and channels in the activated carbon matrix is attributed to the release of volatiles from the precursor material due to the dehydrating effect of  $\text{ZnCl}_2$  at elevated temperature. However, these pores are unstable and tend to collapse or enlarge at higher temperature, thereby reducing the surface area of the activated carbon.

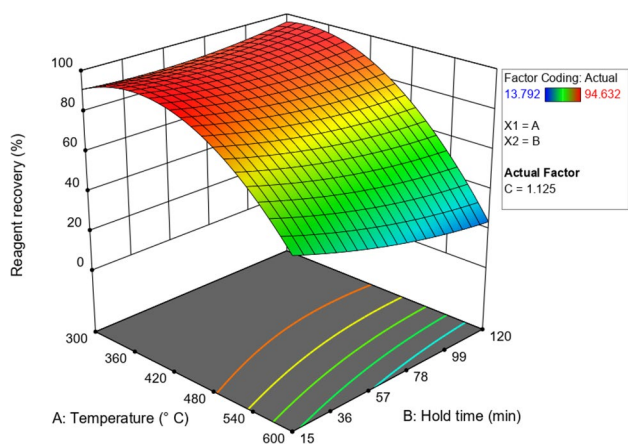


**Fig. 3** Interaction effects of temperature and hold time on reagent recovery for chemically activated carbons derived from peanut shells

The one factor effect on the surface area is shown in Fig. S4, see Supplementary Information. The surface area considerably increases with increase in temperature to ~520 °C and a decrease in microporosity is noted with further increase in temperature > 520 °C. Microporosity starts to decrease at I.R. > 1. This is associated with widening of the pores with increase in ZnCl<sub>2</sub> loading, which leads to increased mesoporosity, as shown in Figs. S5 and S6 (see Supplementary Information). The surface area remains below 500 m<sup>2</sup>/g with carbonisation temperature < 375 °C, within the selected range of I.R. However, at I.R. > 1 and carbonisation temperature > 420 °C, the surface area increased considerably above 500 m<sup>2</sup>/g.

Increasing porosity with increasing I.R. suggests that porosity is created by the interstices left in the carbon material after washing and, at these temperatures, volatile substances are released from the surface of the carbon material during carbonisation. Figure 2b shows the effect of the interaction of temperature and I.R. on porosity development. The above discussion stated the most significant activation parameters (temperature and I.R.) and the range of temperatures and I.R. for producing activated carbons with diverse

properties from peanut shells for various applications, which was lacking from the previous studies using the same precursor.

Reagent recovery (R.R.) from the activation process primarily depends on two factors (temperature and hold time). As shown in Fig. 3, the R.R. demonstrates a significant decrease with carbonisation temperature above 500 °C. This is likely associated with the reagent evaporating from the carbon sample as the temperature increases. It is also noted that R.R. decreases as hold time increases with temperature, ascribed to the fact that more evaporation is expected the longer the activating agent stays at higher temperatures.

Sample densities were observed to increase with an increase in both temperature and I.R. The increase in density with I.R. may be linked to tar inhibition by ZnCl<sub>2</sub> resulting from the condensation reaction [22]. As shown in Table S4 (see Supplementary Information), all activated carbon samples show relatively high densities with the minimum being 1.455 g/cm<sup>3</sup> and maximum, 1.750 g/cm<sup>3</sup>.

### Activation Process Optimisation

It was observed that there is a trade-off between yield and surface area; therefore, the Design Expert desirability function was employed to reach a balance. In the optimisation process, a target was set for the yield while the surface area was maximised. Design of experiments suggests optimisation of the produced carbon, to give a relatively high surface area of 1662 m<sup>2</sup>/g and yield of 45.93% with the following activation parameters: a temperature of 600 °C, a hold time of 15 min, and an I.R. of 2. Experimental validation was performed, in triplicate, to ascertain the optimal conditions produced by RSM. Table 4 presents the optimised activation parameters from RSM and the validations obtained via experiment, note these samples (PNTS1.7-485-15) were used for further characterisation with PNTS2-600-15. As shown in Table 4, the optimised sample shows an average surface area of 1687 m<sup>2</sup>/g, which is relatively higher than the quantity previously recorded for biochars created using the same precursor.

**Table 4** Optimal activation conditions to produce high carbon yield and surface area for chemically activated carbons derived from peanut shells, and experimental validation

Source	Activation parameters			Responses		Desirability	Avg. Pore size, nm
	Temp., °C	Hold time, min	Impregnation ratio, I.R., wt/wt	Yield, %	Surface area, m <sup>2</sup> /g		
RSM	485	15	1.7	47.22	1727	1	
Validation experiment 1	485	15	1.7	47.41	1683		3
Validation experiment 2	485	15	1.7	46.88	1696		3
Validation experiment 3	485	15	1.7	46.80	1683		3

**Table 5** Textural characteristics of the prepared activated carbon and experimental design with the response variables (yield and surface area) for chemically activated carbons derived from peanut shells

Run	Sample name	A			B			C			Dependent variables	
		Temp., °C	Hold time, min.	I.R. (wt/wt)	Avg. Pore size, nm	Micropore vol., cm <sup>3</sup> /g	Total pore vol., cm <sup>3</sup> /g	Yield (Y <sub>1</sub> ), %	Surface area (Y <sub>2</sub> ), m <sup>2</sup> /g			
1	PNTS1.13-450-120	450	120	1.13	3	0.416	0.876	46.63	1562			
2	PNTS1.13-300-68	300	68	1.13	6	0.006	0.006	60.20	51			
3	PNTS1.13-450-68	450	68	1.13	3	0.431	0.810	48.94	1464			
4	PNTS0.25-600-120	600	120	0.25	3	0.247	0.283	45.55	537			
5	PNTS1.13-450-68	450	68	1.13	3	0.407	0.787	48.95	1420			
6	PNTS0.25-300-120	300	120	0.25	43	Negligible	0.006	64.07	Negligible			
7	PNTS2-300-15	300	15	2	8	Negligible	0.001	61.01	1			
8	PNTS0.25-300-15	300	15	0.25	25	Negligible	Negligible	64.99	Negligible			
9	PNTS1.13-450-68	450	68	1.13	3	0.429	0.857	48.73	1539			
10	PNTS2-600-15	600	15	2	3	0.276	1.016	45.93	1662			
11	PNTS0.25-450-68	450	68	0.25	3	0.224	0.274	49.87	586			
12	PNTS0.25-600-15	600	15	0.25	3	0.248	0.290	46.20	550			
13	PNTS1.13-450-15	450	15	1.13	3	0.416	0.746	49.03	1349			
14	PNTS2-300-120	300	120	2	3	0.025	0.047	57.33	84			
15	PNTS2-600-120	600	120	2	3	0.278	0.861	45.93	1510			
16	PNTS1.13-450-68	450	68	1.13	3	0.443	0.854	48.21	1541			
17	PNTS2-450-68	450	68	2	3	0.351	0.875	46.90	1551			
18	PNTS1.13-600-68	600	68	1.13	2	0.391	0.687	44.23	1262			
Optimised	PNTS1.7-485-15	485	15	1.7	3	0.387	0.940	47.41	1683			

## Characterisation Analysis

Table S4 (see Supplementary Information) and Table 5 present the surface area, average pore size, micropore volume, yield, micropore area, and mesopore area (external surface area) obtained from the textural analysis of all AC samples through N<sub>2</sub> adsorption. The total pore volume was calculated from the N<sub>2</sub> adsorption data using Eq. (3). The N<sub>2</sub> adsorption – desorption isotherms of PNTS2-600-15 and PNTS1.7-485-15 are shown in Fig. S7 (see Supplementary Information); it can be observed that both samples are characterised by a mixture of micro- and mesopores (as seen by the opening of the knee). However, the isotherm of PNTS1.7-485-15 is approaching a horizontal plateau which indicates the presence of uniform wider micropores; by contrast, the plateau of PNTS2-600-15 continues at high relative pressure (P/P<sub>0</sub>) and the presence of hysteresis indicates higher mesopore volume. The pore size distribution (PSD), as shown in Fig. S8 (see Supplementary Information), shows that both samples are characterised by pore size < 50 nm. It can be observed that PNTS2-600-15 exhibits a more heterogenous characteristic due to the presence of various pore sizes, as shown in the PSD.

As discussed by Seader et al. [38], the high capacity of a sorbent which helps to minimize the amount of sorbent used in a system is one of the properties that make a sorbent suitable for commercial use.

A relatively high surface area of 1662 m<sup>2</sup>/g was achieved from the design of experiment, and the lowest value < 1 m<sup>2</sup>/g. The low surface area was a result of low I.R. and activation temperature. It is observed that at high temperature and I.R. of 1.13, more micropore area is produced with the highest being 849 m<sup>2</sup>/g. Depending on the adsorbate molecule size, micropore volume has a higher effect than the mesopore volume in liquid adsorption. Micropore volume favours adsorption of micropollutant in a liquid phase adsorption [39]. Thus, these samples with high micropore volume can take advantage in a liquid adsorption, provided the adsorbate molecules are small enough to be accommodated with the micropores. Table 5 shows that all samples have average pore size > 2 nm, and are, therefore, classified as mesoporous [40].

Figure 4 shows the scanning electron micrographs obtained for the parent material and two activated carbon samples. As shown in Fig. 4a, the raw PNTS sample exhibits a rough and irregular cellular structure with no visible openings within



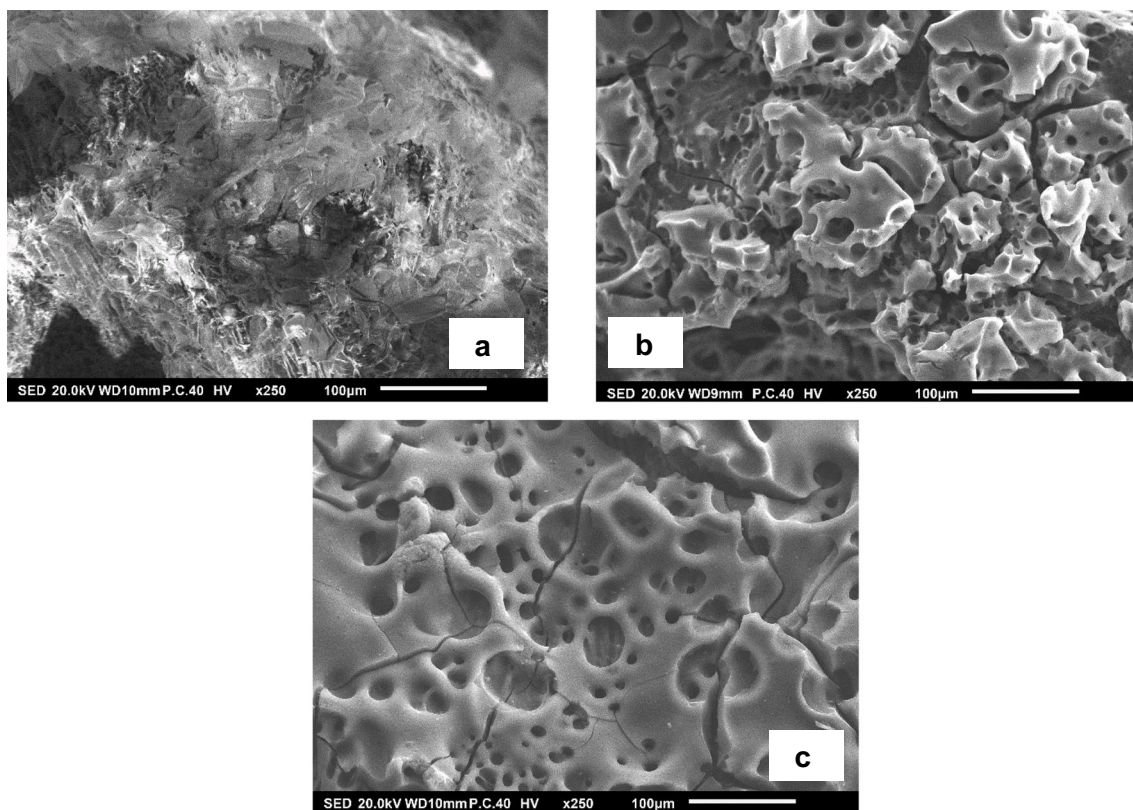


**Fig. 4** Scanning electron micrographs of **a** raw peanut shells (PNTS), and for chemically activated carbons derived from peanut shells: **b** PNTS1.7-485-15 and **c** PNTS2-600-15

the structure. However, after activation, at low magnification (250x), clear channels are visible within the structure, as shown in Fig. 4b and c. The images show the geometrical heterogeneity of the activated carbon materials, coupled with the pore characteristics shown in Table 5, this will contribute to the unique sorption properties of the activated carbon materials [41]. The surface of the optimised sample (PNTS1.7-485-15) is comparatively smooth and textural analysis (Table 5) demonstrates the presence of both micro- and mesopores within the carbon. At the same magnification, the surface of run 10 (PNTS2-600-15) appears to be smoother and but with the presence of larger channels, which can be attributed to the widening of the pores, with an increase in  $\text{ZnCl}_2$  loading, which leads to increased mesopore area (Table 5).

The micropore character for the optimised materials was also visualised using Dubinin-Radushkevich analysis (Figs. S9 and S10, see Supplementary Information), which showed that the microporosity deviates from a Gaussian distribution with more filling at larger pore widths, indicating that the microporosity present is predominantly comprised of supermicropores. In tandem with the micropore contribution to the total pore volume, shown in Table 5, this is likely a key contribution to the small average pore diameters observed for these materials.

Figure 5a shows the PZC plot for the optimal runs PNTS2-600-15 and PNTS1.7-485-15. The PZC was 5.8 for PNTS2-600-15 and 4.58 for the optimised sample. PZC plays a significant role in the selection of adsorbents for an adsorption system. When the pH of a solution ( $\text{pH}_{\text{solution}}$ ) is lower than the PZC of an adsorbent, the surface of the adsorbent becomes positively charged due to protonation of the acidic groups present on the surface and when  $\text{pH}_{\text{solution}}$  above the PZC of an adsorbent, the surface of the adsorbent becomes negatively charged because of the dissociation or ionisation of the acidic oxygen groups on the surface [42]. This can affect the interaction of the adsorbent surface and charged species, such as ionic dyes.

Surface chemistry was further probed using FTIR analysis. Various peaks in the FTIR spectrum of the precursor (Fig. 5b) indicate the presence of several functional groups in the raw peanut shell. The absorption peaks at  $3332\text{ cm}^{-1}$  and  $1249\text{ cm}^{-1}$  correspond to the O-H stretching frequency ( $3600\text{--}3200\text{ cm}^{-1}$ ) and bending frequency ( $1410\text{--}1260$ ), respectively [43], and this could be associated with the presence of cellulose and water of crystallisation [26, 43]. It is observed that the O-H stretching disappeared in the activated samples, which could be attributed to the dehydrating effects of  $\text{ZnCl}_2$  and increased activation temperature. The absorption

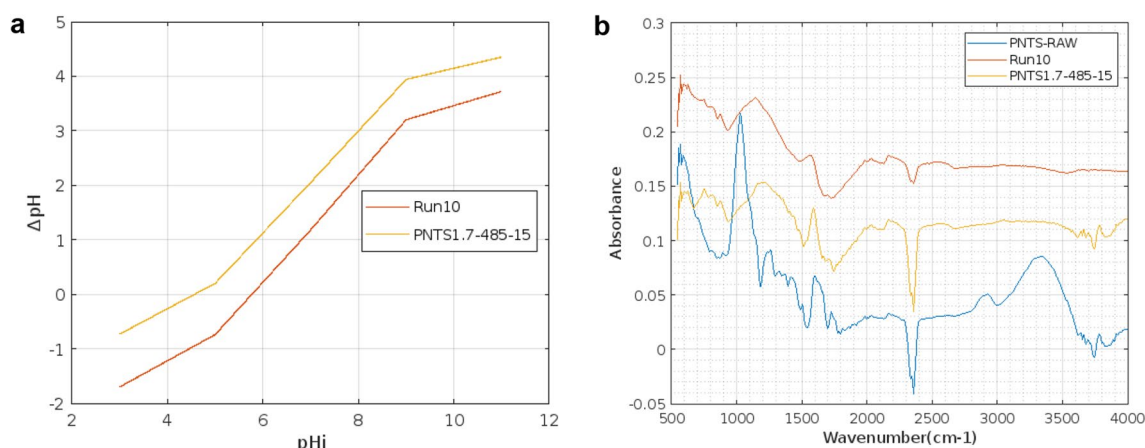


**Fig. 5** **a** Point of zero charge plots obtained for chemically activated carbons derived from peanut shells: PNTS2-600-15 and PNTS1.7-485-15; **b** FTIR spectra for raw PNTS, and for chemically activated carbons derived from peanut shells: PNTS2-600-15 and PNTS1.7-485-15

**Table 6** Proximate Analysis of raw peanut shells, and for chemically activated carbons derived from peanut shells: PNTS2-600-15 and PNTS1.7-485-15

	RAW PNTS	PNTS2-600-15	PNTS1.7-485-15
Volatile matter (%)	69.79	6.53	11.40
Fixed carbon (%)	27.53	91.19	86.42
Moisture content (%)	1.71	1.67	2.03
Ash (%)	< 1	< 1	< 0.5

peaks at  $1728\text{ cm}^{-1}$  and  $1712\text{ cm}^{-1}$ , for the raw and optimal run samples, indicate the presence of carbonyl ( $\text{C}=\text{O}$ ) stretching vibrations of carboxyl groups [26]. N-H bending, which can be associated with amine functional groups ( $1650\text{--}1560\text{ cm}^{-1}$ ) is observed to be present in all samples. The bands at  $1026\text{ cm}^{-1}$ ,  $1141\text{ cm}^{-1}$  and  $1188\text{ cm}^{-1}$  could be attributed to the C-O contributions from acid anhydride groups. This indicates that the surface of the carbon is heterogeneous in character and would likely enhance adsorption of polar species.

**Table 7** Comparison of MO removal efficiency with various adsorbents

Adsorbent	% Removal	Experimental conditions				References
		Adsorbent dose (g/L)	pH	temp. ( $^{\circ}\text{C}$ )	time (hr)	
AC from popcorn	48.5	0.25	-	25	12	[45]
AC from waste tire rubber	80.0	0.5	3.60	23	24	[46]
AC from coconut shell	100	10	-	25	0.2	[47]
Mesoporous carbon from Silica material	99.0	2.0	-	25	1	[48]
AC from grape seed	94.0	20	2.0	45	55 min	[49]
AC/ $\text{NiFe}_2\text{O}_4$	99	3.0	3.0	30	30 min	[50]
PNTS2-600-15	99.8	1.0	5.5	22	24	This work

Proximate analysis provides insight into the moisture, volatile, fixed carbon, and ash contents of carbon samples, and the data obtained for the raw PNTS, and optimal runs are shown in Table 6. The moisture and ash contents are < 3% and 1% respectively, for all samples. The low ash content is an indication of quality carbon material, and this makes the AC potentially suitable for the removal of organic pollutant from an aqueous phase due to their hydrophobic nature [44]. Low volatile content is observed in PNTS2-600-15, and this can be attributed to the degree of heat treatment during carbonisation i.e., most volatiles were released from the surface of the carbon during carbonisation.

## Adsorption Test

Figure S11 (see Supplementary Information) presents the percentage removal of MO with respect to time, under constant initial concentration, and solution pH. The results indicate that the rate of MO removal increases with contact time. The uptake of MO with Run 10 (PNTS2-600-15) occurs faster; this can be attributed to the fact that run 10

is characterised with larger mesopore area (Table 5), which aids the diffusion of the MO species into the interior sites of the adsorbent. However, after 24 h contact time, both samples attained nearly the same percentage removal. Table 7 lists the MO removal efficiency of some adsorbent materials previously reported [45–50]. It can be seen from the table, in terms of the removal efficiency, that the adsorbent material developed within this study shows excellent performance.

## Conclusion

The results presented within this investigation show that the chemical activation method employed was suitable for creating peanut shell based activated carbon, as relatively large surface areas were recorded. The RSM reveals that temperature and impregnation ratio were the most important parameters that influenced the AC properties. The AC samples show heterogenous morphology and functional groups, which may enhance their adsorption capacity for various pollutants. This work suggests that peanut shell is a promising raw material for producing effective adsorbents for wastewater treatment. Future work will focus on the adsorption performance and optimization of the AC samples for the removal of different contaminants.

**Supplementary Information** The online version contains supplementary material available at <https://doi.org/10.1007/s12155-023-10683-7>.

**Acknowledgements** The authors express sincere gratitude to the National Physical Laboratory (NPL) for conducting the density measurements that are presented in this work.

## Declarations

**Conflict of Interest** The authors declare no competing interests.

**Open Access** This article is licensed under a Creative Commons Attribution 4.0 International License, which permits use, sharing, adaptation, distribution and reproduction in any medium or format, as long as you give appropriate credit to the original author(s) and the source, provide a link to the Creative Commons licence, and indicate if changes were made. The images or other third party material in this article are included in the article's Creative Commons licence, unless indicated otherwise in a credit line to the material. If material is not included in the article's Creative Commons licence and your intended use is not permitted by statutory regulation or exceeds the permitted use, you will need to obtain permission directly from the copyright holder. To view a copy of this licence, visit <http://creativecommons.org/licenses/by/4.0/>.

## References

- INC (2020) Nuts and dried fruits statistical yearbook 2019/2020. International Nut and Dried Fruit Council Spain. Publications - International Nut & Dried Fruit Council <https://www.nutfruit.org>. Accessed 21 Apr 2023
- Perea-Moreno M-A, Manzano-Agugliaro F, Hernandez-Escobedo Q, Perea-Moreno A-J (2018) Peanut shell for energy: properties and its potential to respect the environment. Sustainability 10:3254. <https://doi.org/10.3390/su10093254>
- Malik R, Ramteke D, Wate S (2006) Physico-chemical and surface characterization of adsorbent prepared from groundnut shell by ZnCl<sub>2</sub> activation and its ability to adsorb colour. Indian J Chem Technol 13. <http://nopr.niscares.in/handle/123456789/7048>. Accessed 03 Mar 2022
- Titirici M-M, White RJ, Brun N, Budarin VL, Su DS, Del Monte F, Clark JH, Maclachlan MJ (2015) Sustainable carbon materials. Chem Soc Rev 44:250–290. <https://doi.org/10.1039/C4CS00232F>
- Heidarinejad Z, Dehghani MH, Heidari M, Javedan G, Ali I, Sil-lanpää M (2020) Methods for preparation and activation of activated carbon: a review. Environ Chem Lett 18:393–415. <https://doi.org/10.1007/s10311-019-00955-0>
- Seader J, Henley EJ, Roper DK (2016) Separation process principles: With applications using process simulators. Wiley, Hoboken
- Klasson KT, Ledbetter CA, Uchimiya M, Lima IM (2013) Activated biochar removes 100% dibromochloropropane from field well water. Environ Chem Lett 11:271–275. <https://doi.org/10.1007/s10311-012-0398-7>
- Dai Y, Sun Q, Wang W, Lu L, Liu M, Li J, Yang S, Sun Y, Zhang K, Xu J (2018) Utilizations of agricultural waste as adsorbent for the removal of contaminants: a review. Chemosphere 211:235–253. <https://doi.org/10.1016/j.chemosphere.2018.06.179>
- Kumari G, Soni B, Karmee SK (2020) Synthesis of activated carbon from groundnut shell via chemical activation. J Inst Eng India Ser E 1–8. <https://doi.org/10.1007/s40034-020-00176-z>
- Kamaraj M, Umamaheswari P (2017) Preparation and characterization of Groundnut shell activated carbon as an efficient adsorbent for the removal of Methylene blue dye from aqueous solution with microbiostatic activity. J Mater Environ Sci 8:2019–2025
- Ahmad MA, Yusop MFM, Zakaria R, Karim J, Yahaya NKE, Yusoff MaM, Hashim NHF, Abdullah NS (2021) Adsorption of methylene blue from aqueous solution by peanut shell based activated carbon. Mater Today Proc 47:1246–1251. <https://doi.org/10.1016/j.matpr.2021.02.789>
- Garg D, Kumar S, Sharma K, Majumder C (2019) Application of waste peanut shells to form activated carbon and its utilization for the removal of Acid Yellow 36 from wastewater. Groundw Sustain Dev 8:512–519. <https://doi.org/10.1016/j.gsd.2019.01.010>
- Malik R, Ramteke DS, Wate SR (2007) Adsorption of malachite green on groundnut shell waste based powdered activated carbon. Waste Manag 27:1129–1138. <https://doi.org/10.1016/j.wasman.2006.06.009>
- Sricharoenchaikul V, Pechyen C, Aht-Ong D, Atong D (2008) Preparation and characterization of activated carbon from the pyrolysis of physic nut (*Jatropha curcas* L.) waste. Energy Fuels 22:31–37. <https://doi.org/10.1021/ef700285u>
- Caturla F, Molina-Sabio M, Rodriguez-Reinoso F (1991) Preparation of activated carbon by chemical activation with ZnCl<sub>2</sub>. Carbon 29:999–1007. [https://doi.org/10.1016/0008-6223\(91\)90179-M](https://doi.org/10.1016/0008-6223(91)90179-M)
- Smíšek M, Černý S (1970) Active carbon: manufacture, properties and applications. Elsevier Publishing Company, Amsterdam
- Hock PE, Zaini MaA (2018) Activated carbons by zinc chloride activation for dye removal – a commentary. Acta Chim Slovaca 11:99–106. <https://doi.org/10.2478/acs-2018-0015>
- Anisuzzaman S, Joseph CG, Krishnaiah D, Bono A, Suali E, Abang S, Fai L (2016) Removal of chlorinated phenol from aqueous media by guava seed (*Psidium guajava*) tailored activated carbon. Water Resour Ind 16:29–36. <https://doi.org/10.1016/j.wri.2016.10.001>
- Molina-Sabio M, Rodriguez-Reinoso F (2004) Role of chemical activation in the development of carbon porosity. Colloids Surf a

- Physicochem Eng Asp 241:15–25. <https://doi.org/10.1016/j.colsurf.2004.04.007>
20. Jawad AH, Alkarkhi AF, Mubarak NSA (2015) Photocatalytic decolorization of methylene blue by an immobilized TiO<sub>2</sub> film under visible light irradiation: optimization using response surface methodology (RSM). *Desalin Water Treat* 56:161–172. <https://doi.org/10.1080/19443994.2014.934736>
  21. Mehmood T, Ahmed A, Ahmad A, Ahmad MS, Sandhu MA (2018) Optimization of mixed surfactants-based  $\beta$ -carotene nanoemulsions using response surface methodology: an ultrasonic homogenization approach. *Food Chem* 253:179–184. <https://doi.org/10.1016/j.foodchem.2018.01.136>
  22. Ahmadpour A, Do D (1997) The preparation of activated carbon from macadamia nutshell by chemical activation. *Carbon* 35:1723–1732. [https://doi.org/10.1016/S0008-6223\(97\)00127-9](https://doi.org/10.1016/S0008-6223(97)00127-9)
  23. Ruiz Bevia F, Prats Rico D, Marcilla Gomis A (1984) Activated carbon from almond shells. Chemical activation. 1. Activating reagent selection and variables influence. *Ind Eng Chem Prod Res Dev* 23:266–269
  24. Zhang H, Yan Y, Yang L (2010) Preparation of activated carbon from sawdust by zinc chloride activation. *Adsorption* 16:161–166. <https://doi.org/10.1007/s10450-010-9214-5>
  25. Pabari RM, Ramtoola Z (2012) Application of face centred central composite design to optimise compression force and tablet diameter for the formulation of mechanically strong and fast disintegrating orodispersible tablets. *Int J Pharm* 430:18–25. <https://doi.org/10.1016/j.ijpharm.2012.03.021>
  26. Saygılı H, Güzel F (2016) High surface area mesoporous activated carbon from tomato processing solid waste by zinc chloride activation: process optimization, characterization and dyes adsorption. *J Clean Prod* 113:995–1004. <https://doi.org/10.1016/j.jclepro.2015.12.055>
  27. Ottaway M (1982) Use of thermogravimetry for proximate analysis of coals and cokes. *Fuel* 61:713–716. [https://doi.org/10.1016/0016-2361\(82\)90244-7](https://doi.org/10.1016/0016-2361(82)90244-7)
  28. Bakatula EN, Richard D, Neculita CM, Zagury GJ (2018) Determination of point of zero charge of natural organic materials. *Environ Sci Pollut Res* 25:7823–7833. <https://doi.org/10.1007/s11356-017-1115-7>
  29. Brunauer S, Emmett PH, Teller E (1938) Adsorption of gases in multimolecular layers. *J Am Chem Soc* 60:309–319. <https://doi.org/10.1021/ja01269a023>
  30. De Boer J, Lippens B, Linsen B, Broekhoff J, Van Den Heuvel A, Osinga TJ (1966) Thet-curve of multimolecular N<sub>2</sub>-adsorption. *J Colloid Interface Sci* 21:405–414. [https://doi.org/10.1016/0095-8522\(66\)90006-7](https://doi.org/10.1016/0095-8522(66)90006-7)
  31. Barrett EP, Joyner LG, Halenda PP (1951) The determination of pore volume and area distributions in porous substances. I. computations from nitrogen isotherms. *J Am Chem Soc* 73:373–380. <https://doi.org/10.1021/ja01145a126>
  32. Noordin MY, Venkatesh V, Sharif S, Elting S, Abdullah A (2004) Application of response surface methodology in describing the performance of coated carbide tools when turning AISI 1045 steel. *J Mater Process Technol* 145:46–58. [https://doi.org/10.1016/S0924-0136\(03\)00861-6](https://doi.org/10.1016/S0924-0136(03)00861-6)
  33. Ahmadi M, Vahabzadeh F, Bonakdarpour B, Mofarrah E, Meheranian M (2005) Application of the central composite design and response surface methodology to the advanced treatment of olive oil processing wastewater using Fenton's peroxidation. *J Hazard Mater* 123:187–195. <https://doi.org/10.1016/j.jhazmat.2005.03.042>
  34. Vining G (2010) Technical advice: residual plots to check assumptions. *Qual Eng* 23:105–110. <https://doi.org/10.1080/08982112.2011.535696>
  35. Miller DM (1984) Reducing transformation bias in curve fitting. *Am Stat* 38:124–126. <https://doi.org/10.1080/00031305.1984.10483180>
  36. El-Masry E, Ibrahim H, Moamen OA, Zaher W (2022) Sorption of some rare earth elements from aqueous solutions using copolymer/activated carbon composite: multivariate optimization approach. *Adv Powder Technol* 33:103467. <https://doi.org/10.1016/j.apt.2022.103467>
  37. Donald J, Ohtsuka Y, Xu CC (2011) Effects of activation agents and intrinsic minerals on pore development in activated carbons derived from a canadian peat. *Mater Lett* 65:744–747. <https://doi.org/10.1016/j.matlet.2010.11.049>
  38. Seader JD, Henley EJ, Roper DK (2010) *Separation Process Principles*, 3rd edn. John Wiley Incorporated, Hoboken
  39. Murray A, Örmeci B (2018) Competitive effects of humic acid and wastewater on adsorption of Methylene Blue dye by activated carbon and non-imprinted polymers. *J Environ Sci* 66:310–317. <https://doi.org/10.1016/j.jes.2017.04.029>
  40. Thommes M, Kaneko K, Neimark AV, Olivier JP, Rodriguez-Reinoso F, Rouquerol J, Sing KS (2015) Physisorption of gases, with special reference to the evaluation of surface area and pore size distribution (IUPAC Technical Report). *Pure Appl Chem* 87:1051–1069. <https://doi.org/10.1515/pac-2014-1117>
  41. Dąbrowski A, Podkościelny P, Hubicki Z, Barczak M (2005) Adsorption of phenolic compounds by activated carbon—a critical review. *Chemosphere* 58:1049–1070. <https://doi.org/10.1016/j.chemosphere.2004.09.067>
  42. Tran HN, You S-J, Chao H-P (2016) Effect of pyrolysis temperatures and times on the adsorption of cadmium onto orange peel derived biochar. *Waste Manag Res* 34:129–138. <https://doi.org/10.1177/0734242X15615698>
  43. Fleming I, Williams DH (1966) *Spectroscopic methods in organic chemistry*. Springer, Berlin
  44. Zuim DR, Carpiné D, Distler GaR, De Paula Scheer A, Igarashi-Mafra L, Mafra MR (2011) Adsorption of two coffee aromas from synthetic aqueous solution onto granular activated carbon derived from coconut husks. *J Food Eng* 104:284–292. <https://doi.org/10.1016/j.jfoodeng.2010.12.019>
  45. Yu Y, Qiao N, Wang D, Zhu Q, Fu F, Cao R, Wang R, Liu W, Xu B (2019) Fluffy honeycomb-like activated carbon from popcorn with high surface area and well-developed porosity for ultra-high efficiency adsorption of organic dyes. *Bioresour Technol* 285:121340. <https://doi.org/10.1016/j.biortech.2019.121340>
  46. Islam MT, Saenz-Arana R, Hernandez C, Guinto T, Ahsan MA, Bragg DT, Wang H, Alvarado-Tenorio B, Noveron JC (2018) Conversion of waste tire rubber into a high-capacity adsorbent for the removal of methylene blue, methyl orange, and tetracycline from water. *J Environ Chem Eng* 6:3070–3082. <https://doi.org/10.1016/j.jece.2018.04.058>
  47. Islam MS, Ang BC, Gharehkhani S, Afifi ABM (2016) Adsorption capability of activated carbon synthesized from coconut shell. *Carbon Lett* 20:1–9. <https://doi.org/10.5714/CL.2016.20.001>
  48. Mohammadi N, Khani H, Gupta VK, Amerah E, Agarwal S (2011) Adsorption process of methyl orange dye onto mesoporous carbon material—kinetic and thermodynamic studies. *J Colloid Interf Sci* 362:457–462. <https://doi.org/10.1016/j.jcis.2011.06.067>
  49. Yönten V, Sanyürek NK, Kivanç MR (2020) A thermodynamic and kinetic approach to adsorption of methyl orange from aqueous solution using a low cost activated carbon prepared from *Vitis vinifera* L. *Surf Interfaces* 20:100529. <https://doi.org/10.1016/j.surfin.2020.100529>
  50. Jiang T, Liang Y-D, He Y-J, Wang Q (2015) Activated carbon/NiFe<sub>2</sub>O<sub>4</sub> magnetic composite: a magnetic adsorbent for the adsorption of methyl orange. *J Environ Chem Eng* 3:1740–1751. <https://doi.org/10.1016/j.jece.2015.06.020>

**Publisher's Note** Springer Nature remains neutral with regard to jurisdictional claims in published maps and institutional affiliations.